

Modelling the Binding of FimH to Carbon Nano-dots and the Fluorescence Intensity of the Bound Molecules for Bacteria Detection

05 Fluoretiq

Luca Bennett, Maria Jenkins, Vedang Joshi, Mark Crowley and Mark Toolan

EMAT30005 Mathematical and Data Modelling

Department of Engineering Mathematics, University of Bristol

3rd December 2020

1 Introduction and Background

The fast and accurate diagnosis of infectious diseases is crucial to saving lives and relieving pressure on health services, this being especially important during the current world pandemic. In particular, the average diagnosis for bacterial infections can take up to 2 days, yet 30% - 50% of these diagnoses may still be incorrect [7, 3]. This results in the dangerous over-prescription of antibiotics, which has caused a sharp rise in the level of antibiotic resistance, in addition to other complications such as clinical failure, adverse drug effects and rise in costs for hospitals and patients [5]. One such complication of over-prescription has resulted in the antibiotic resistance of *Clostridium difficile* bacteria; there were an estimated 13,286 *C.difficile* infections in 2018 in the UK of which $\approx 36\%$ required hospitalisations [18]. In this paper, we investigate how the use of fluorescence microscopy can assist in efficiently detecting, identifying and measuring bacteria, and how it can improve the diagnostic process.

Using the properties of fluorescence, a Bristol based start-up called Fluoretiq Limited have developed a Nanoplex™ platform that can be used to diagnose bacterial infections in less than 15 minutes. When light of a particular wavelength is incident on particles, they are temporarily excited to a higher-energy state. As they relax back down to the ground state they release this energy in the form of light, at a different wavelength. The level of excitement, time delay and colour of light emitted can be used to identify which particle is present in the sample, and the intensity of the emitted light can be used to quantify the concentration of the specific particle.

On certain bacteria, there exist appendages called fimbriae and the tips of these fimbriae have fimH proteins which bind to specific glycans in the body to establish an infection [14]. These glycans can be artificially mimicked with specially developed fluorescent carbon nano-dots, which are mixed with a suspected bacterial sample [2]. Then, by separating the bacteria from the sample and exposing them to a light source within a detector, it is possible to identify any bacteria present, and determine how severe the infection is based on the bacterial concentration. In doing this, an informed diagnosis can be made, leading to the correct initial treatment of a bacterial infection.

All code used in this report may be found at <https://github.com/vedang-joshi/MDM3Rep1>.

2 Methodology

We have separated the modelling process into three phases: binding, fluorescence and bacterial enumeration. The first is a chemical stage, the second a quantum process, and the third a proportionality that relates the detected light intensity to bacterial concentration. The fluorescence photokinetics can be further broken down into two methods: one assuming a generic approach which serves to understand the process as a whole; and the other accounting for photobleaching within the system.

2.1 Binding Process

The first stage of the model describes the binding of carbon nano-dots to the fimH protein. This binding process can be modelled as a reversible chemical reaction, from which we can derive a system of differential equations using the law of mass action.



where F is a fimH protein, C is a carbon nano-dot and B is the resulting bound molecule. The constants r_1 and r_{-1} represent the rates of the forwards and backwards reactions respectively. This

equation assumes that there is a 1 : 1 binding ratio between the fimH proteins and carbon nano-dots, such that multivalent binding does not occur. By assuming the case in which multiple carbon nano-dots bind to one fimH, and the case in which multiple fimH bind to one carbon nano-dot to be equally likely, we can approximate the average binding ratio to be 1 : 1 over a large number of reactions.

By applying the law of mass action to eq. 1, the changes of the concentrations of the reactants and products can be modelled as,

$$\frac{df}{dt} = r_{-1}b - r_1fc, \quad (2)$$

$$\frac{dc}{dt} = r_{-1}b - r_1fc, \quad (3)$$

$$\frac{db}{dt} = r_1fc - r_{-1}b, \quad (4)$$

where f is the concentration of fimH, c the concentration of carbon nano-dots and b the concentration of bound molecules.

At time $t = 0$, the initial conditions $f(0) = f_0$, $c(0) = c_0$ and $b(0) = 0$, can be described by the following set of equations:

$$f(t) + b(t) = f_0, \quad (5)$$

$$c(t) + b(t) = c_0, \quad (6)$$

Figure 1 shows the dynamics of the binding process by depicting how the above system of ODEs stabilises. We can see that the concentrations of the reactants and products reach a steady state.

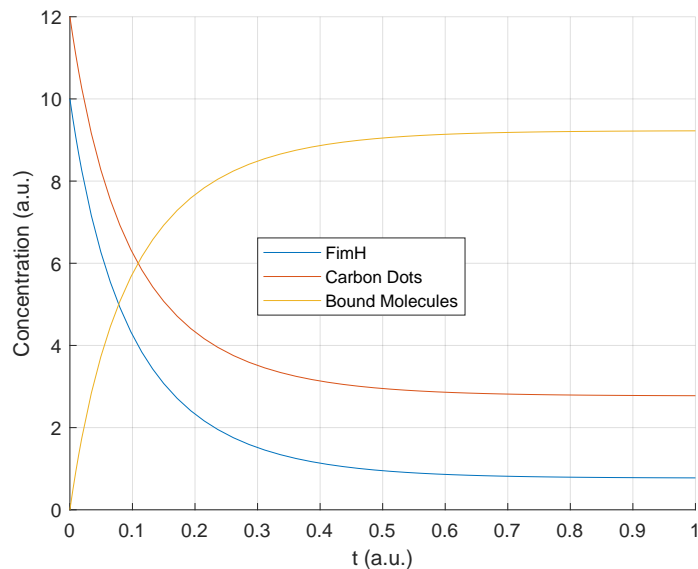


Figure 1: Numerical solution of ODEs in Eq. (2)-(4) assuming $f_0 = 10$, $c_0 = 12$ and $r_1 = 0.5$ and $r_{-1} = 1.1$ (arbitrary constants).

2.2 Fluorescence Photokinetics: A Simple Photocycle Model

Live-cell fluorescence microscopy has allowed researchers to quantify the amount of organisms in any particular solution by studying the kinetics of the fluorescence processes. From this, we can find the exact distribution of the carbon nano-dots within the diagnostic assays. We take inspiration from the law of mass action to develop a simple model of fluorescence and hence, aim to understand the limitations of fluorescence (e.g. photobleaching, explored in section 2.3).

We start with a simple photo-cycle as shown in eq.(7),



where B_n is the non-excited state, B_e is the excited state of the molecule after the binding process with the carbon nano-dots, k_1 is the absorption rate constant and k_{-1} is the fluorescence rate constant. Again, using the law of mass action, we get the following coupled system of ODEs.

$$\frac{db_n}{dt} = -k_1 b_n + k_{-1} b_e, \quad (8)$$

$$\frac{db_e}{dt} = k_1 b_n - k_{-1} b_e, \quad (9)$$

where the absorption constant, k_1 can be defined as the illumination intensity, I_{ex} , multiplied by the absorption cross-section, σ_{ex} , of the fluorescing molecule for the given wavelength of excitation [20], $k_1 = I_{ex} \cdot \sigma_{ex}$. We can relate the absorption cross-section to the molar attenuation coefficient, ϵ , as $\sigma_{ex} = (2303 \cdot \epsilon)/N_A$. In this case, N_A represents Avogadro's number [9]. Solving this coupled system analytically,

$$b_n(t) = \frac{C_2 \cdot k_{-1}}{k_1} - C_1 \cdot e^{-t(k_{-1}+k_1)}, \quad (10)$$

$$b_e(t) = C_2 + C_1 \cdot e^{-t(k_{-1}+k_1)}, \quad (11)$$

where C_1 and C_2 are constants dependent on the initial conditions of the system.

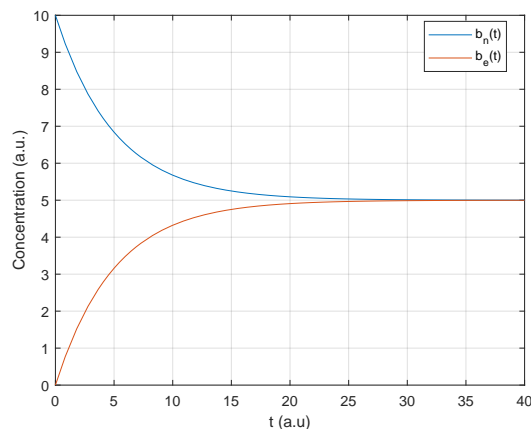


Figure 2: A plot of the solutions to the coupled ODEs in eq.(10)(11) assuming $b_n(0) = 10$, $b_e(0) = 0$, and $k_1 = k_{-1} = 0.1$

It can be seen in figure 2 that $b_n(t)$ and $b_e(t)$ both reach a steady state. The dynamics of the steady states must be analysed to see how they vary for different values of the rate constants k_1 and k_{-1} .

As eq. 7 conserves mass, we can say that $b_n + b_e = b_n(0)$, where $b_n(0)$ is the initial value of $b_n(t)$. Substituting this into eq. 10,

$$\frac{db_n}{dt} = -k_1 b_n + k_{-1}(N - b_n). \quad (12)$$

The steady state values of b_n and b_e can be found by taking $db_n/dt = 0$, hence,

$$b_{n_s} = \frac{k_{-1} b_n(0)}{k_1 + k_{-1}}, \quad (13)$$

$$b_{e_s} = b_n(0) - \frac{k_{-1} b_n(0)}{k_1 + k_{-1}} = \frac{k_1 b_n(0)}{k_1 + k_{-1}}, \quad (14)$$

where b_{n_s} and b_{e_s} are the steady state values of $b_n(t)$ and $b_e(t)$ respectively.//

The steady state values of b_n and b_e can be plotted against varying values of k_1 and k_{-1} to determine the impact of rate constants on the fluorescence intensity (which is related to the steady state value of b_e). It can be seen in figure 3 that when $k_1 \gg k_{-1}$, $b_{n_s} \approx 0$ and $b_{e_s} \approx b_n(0)$, and when $k_{-1} \gg k_1$, $b_{n_s} \approx b_n(0)$ and $b_{e_s} \approx 0$. Hence in order to maximise the intensity of fluorescence detected, the rate of the forward reaction must be much larger than the rate of the backward reaction, k_{-1} , as in this case the steady state value of the concentration of excited molecules is greatest.

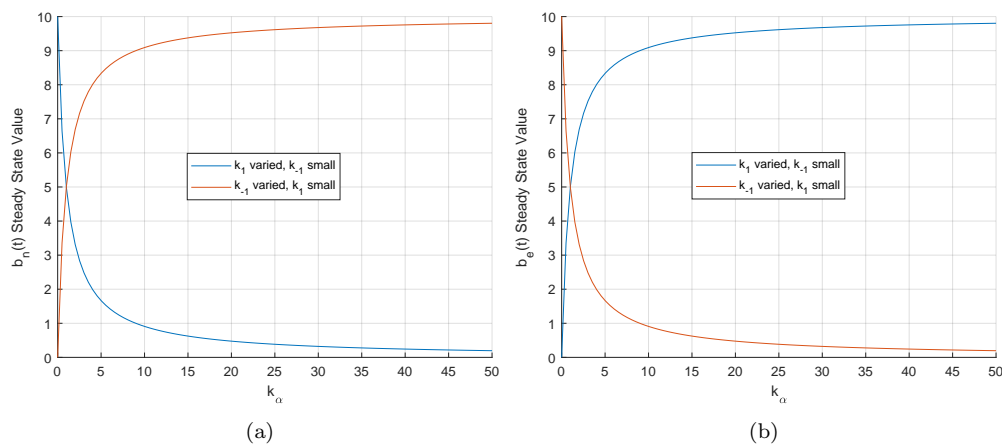
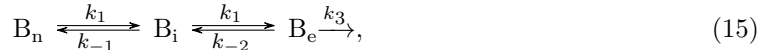


Figure 3: A plot of the steady state values of $b_n(t)$ and $b_e(t)$, (a) and (b) respectively, for varying values of k_1 and k_{-1} , assuming $k_{\pm 1} = 1$ when small and consists of 100 evenly distributed values in the interval $[0, 50]$ when varied.

2.3 Fluorescence Photokinetics: Photobleaching Model

The initial model does not take into account that if the bound excited molecules are exposed to prolonged excitation, they are destroyed. This means that such molecules are irreversibly taken out of the photo-cycle we refer to above. This effect is known as ‘photobleaching’. Photobleaching depletes the bound molecule store so fewer molecules are available for excitation, thereby reducing the observed fluorescence. Evidence for photobleaching during *E.coli* detection has been provided

within the literature on several counts [17, 16], thus it is imperative to represent this behaviour in our subsequent model. We adjust our initial model to add another intermediate step in the photocycle, B_i , and add an irreversible reaction step to the state, B_e , to account for the photobleaching effect. The change of states between the excited state and the intermediate state is called internal conversion [11]. Here we extend the work by Wüstner et al. [20] and we take inspiration from Jablonski's diagram (see Appendix B and [1]) with a ground state, B_n , an intermediate state, B_i , and an excited state, B_e . We can model this system as follows,



where k_1 is the absorption rate constant across the three states, k_{-1} is the fluorescence rate constant, k_{-2} is the internal conversion rate constant and k_3 is the intrinsic bleach rate constant. We justify the use of a single constant k_1 , across the three states, as in Jablonski's diagram of fluorescence, the absorption occurs from state B_n to B_e through state B_i . We obtain the following system of ODEs,

$$\begin{bmatrix} \frac{db_n}{dt} \\ \frac{db_i}{dt} \\ \frac{db_e}{dt} \end{bmatrix} = \begin{bmatrix} -k_1 & k_{-1} & 0 \\ k_1 & -(k_{-1} + k_1) & k_2 \\ k_1 & -k_2 & -k_3 \end{bmatrix} \begin{bmatrix} b_n \\ b_i \\ b_e \end{bmatrix} \quad (16)$$

and then solve this system analytically and simplify the results,

$$b_n(t) = e^{-k_1 t} (C_1 + \int k_{-1} \cdot e^{k_1 t} b_i(t) dt), \quad (17)$$

$$b_i(t) = e^{-t(k_1+k_{-1})} (C_1 + \int e^{t(k_1+k_{-1})} (k_1 b_n(t) + k_{-2} b_e(t)) dt), \quad (18)$$

$$b_e(t) = e^{-t(k_{-2}+k_3)} (C_1 + \int k_{-1} \cdot e^{t(k_{-2}+k_3)} b_i(t) dt), \quad (19)$$

where C_1 is a constant dependant on the initial conditions of the system. We conduct a symbolic eigenvector and eigenvalue analysis on the system presented in Appendix A where the diagonal of the eigenvalues matrix shows the eigenvalues corresponding to the each of the columns of the eigenvectors matrix.

In figure 4, we overlay the fluorescence intensity-time graph (in black) from Pu and Alfano's work [15] on photon emission from stained cancerous tissues to our model of fluorescence. Although Pu and Alfano obtained their results from a different experimental setup to the one used by Fluoretiq, the dynamics of the fluorescence system closely resemble the dynamics of our model (In figure 4 comparing the black and the red curves). Similarly in both graphs, the unexcited particles decay from a starting condition. However, the intermediate state and the excited state particles quickly increasing to a maximum, and then decaying to zero when the photobleaching and fluorescence processes occur. We infer that the concentration and intensity are linked by a constant of proportion. This relationship is investigated further in our next model.

2.4 Fluorescence Photokinetics: Proportionality Model

The intensity of fluorescence detected can be modelled as being directly proportional to the concentration of bound molecules. As the concentration of bound particles reaches a steady state, we use

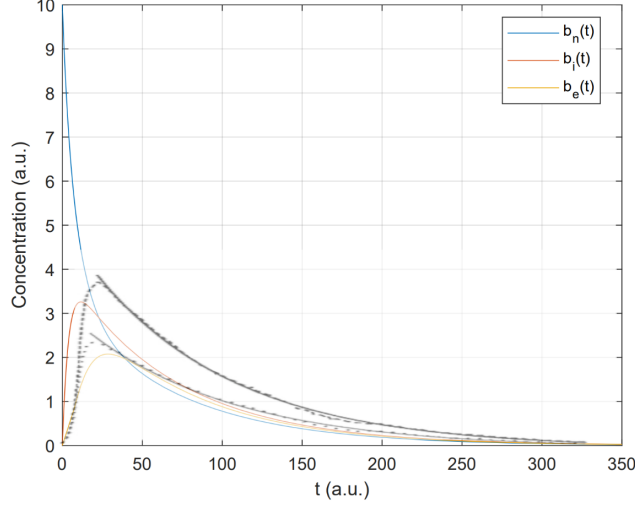


Figure 4: A plot of the solutions for the coupled ODEs shown in eq.(17)-(19) assuming $b_n(0) = 10$, $b_i(0) = 0$, $b_e(0) = 0$ and $k_1 = 0.1$, $k_{-1} = 0.07$, $k_{-2} = 0.08$, $k_3 = 0.01$. The black line overlaid shows the dynamics of fluorescence intensity against time looking at stained cancerous tissues [15].

this steady state value under the assumption that the reaction reached this state before fluorescence occurs.

$$n_{\text{photon}} = \Omega b_s, \quad (20)$$

where n_{photon} is the number of photons detected, Ω is a constant, and b_s is the steady state value of $f(t)$. Using eq. 6,

$$n_{\text{photon}} = \Omega(c_0 - c_s), \quad (21)$$

where c_0 is the initial concentration of carbon nano-dots and c_{steady} is the steady state value of $c(t)$. To estimate parameter Ω we fit our model against data provided by Fluoretiq. The data consists of seven points of carbon nano-dot concentration and the resultant number of photon count events detected. In order to estimate Ω , the model was fitted to the data by minimising the sum squared error. The fit given in figure 5 estimates the value of Ω as $\Omega = 2.3729 \times 10^3$.

2.5 Concentration of Bacteria

As we are taking the steady state values of our ODE we can take $df/dt = 0$, then using eq. 2 & 6,

$$f_s = \frac{r_{-1}b_s}{r_1(c_0 - b_s)}, \quad (22)$$

where f_s is the steady state value of $f(t)$, $b_s = n_{\text{photon}}/\Omega$ from eq. 20.

Hence using eq. 5,

$$f_0 = \frac{n_{\text{photon}}}{\Omega} + \frac{r_{-1}n_{\text{photon}}}{r_1(\Omega c_0 - n_{\text{photon}})}. \quad (23)$$

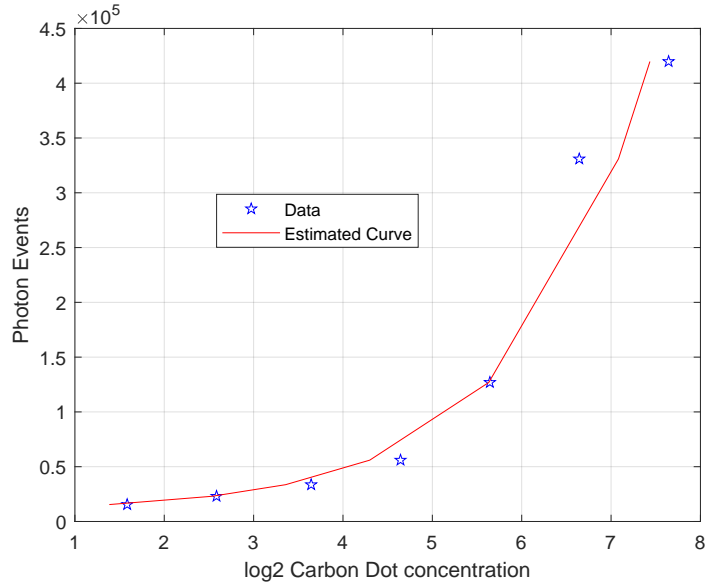


Figure 5: Minimised sum squared error fit of eq. 21 against seven data points to estimate Ω .

The number of bacteria in a sample is simply given by,

$$n_{\text{bact}} = \frac{f_0}{n_{\text{fimH}}}, \quad (24)$$

where n_{bact} is the number of bacteria, f_0 is the initial concentration of fimH, and n_{fimH} is the number of fimH per bacteria. The number of fimbriae containing fimH on an individual *E. coli* ranges from 1 to 1000 [10]. The number of *E. coli* we would find in a sample is sufficient such that we can take the average value of that range. Hence the number of fimH per bacteria can be taken to be $n_{\text{fimH}} = 500$.

The intensity of fluorescence detected is related to the number of photons detected via the relation [6],

$$I = \frac{n_{\text{photon}} h v}{A t}, \quad (25)$$

where I is the intensity of detected fluorescence, h is Planck's constant, v is the frequency of detected fluorescence, A is the area of the detector, and t is the integration time. Hence for a given value of detected intensity, the number of bacteria can be calculated in the case that all the constants are known.

3 Discussion

3.1 Noise

There are a few factors in the measurement of fluorescence intensity that can contribute towards noise in the data. The most significant of these is the autofluorescence of naturally occurring fluorophores in urine, which contributes towards the overall photon count. Fluorophore concentration varies between individuals due to diet [12], and consumption of vitamin supplements [13]. Taking a fluorescence measurement for a control sample with no carbon nano-dots will give a background

photon count, which can be subtracted from the overall photon count of the analysed sample. This ensures the reading is not inflated due to this background noise.

The measurement of photon count, is limited by the stochastic nature of photon emission, the photon noise, which follows a Poisson distribution with mean equal to the square root of the photon count. There are three principle types of noise which contribute to our model: photon noise, read noise (due to the measurement error of the equipment), and dark noise (due to electron excitement by thermal energy). Fortunately, for high values of photon counts, such as the cases considered in our model, read noise and dark noise become negligible and photon noise dominates [4]. This means that we can instead estimate the photon noise of our system, M_{photon} , to follow a Gaussian distribution [19],

$$M_{\text{photon}} \sim \mathcal{N}(\sqrt{\bar{n}_{\text{photon}}}, \sqrt{\bar{n}_{\text{photon}}}). \quad (26)$$

Since we take two readings, one for the background fluorescence and one for the main reading there will be two distributions with different means and variances. Combining these models by subtracting their means and adding their variances will give us a Gaussian distribution for the overall noise of the system.

$$M_{\text{total}} \sim \mathcal{N}(\sqrt{\bar{n}_{\text{photonCD}}} - \sqrt{\bar{n}_{\text{photonAF}}}, \sqrt{\bar{n}_{\text{photonCD}}} + \sqrt{\bar{n}_{\text{photonAF}}}) \quad (27)$$

where n_{photonCD} denotes the photon count in a sample with carbon nano-dots added and n_{photonAF} denotes the photon count in control sample.

Modelling the noise is especially important when performing statistical analysis on the results. This distribution allows us to assess whether the measured fluorescence intensity is sufficient to diagnose the patient positive for a specific infection, or deduce whether further testing is necessary.

3.2 Rates of Reaction

We can deduce that a high rate of forward reaction in eq. (2)-(4) is favourable as the time taken to bind the carbon nano-dots and the fimH is shorter yet they will all still bind. We can increase the rate of reaction in several different ways. We can increase the temperature of the reaction conditions, which will lead to more collisions and hence, more binding of the reactants. Alternatively, we could increase the concentrations of the reactants [8].

Increasing the concentration of the reactants will result in more effective collisions per unit time which is effectively the rate of the reaction. For the set of equations representing the binding process of the reactants, we can increase the initial concentrations of both fimH proteins and the carbon nano-dots to see what effect this has on the speed of the reaction.

We can see that the rate of reaction in figure 6 is relatively faster than that of the reaction modelled in figure 1, as the concentrations have a further decrease in the same amount of time than with the lower starting concentrations. Concentration is also proportional to fluorescence intensity, so on balance, a high starting concentration for both of the reactants will maximise the time efficiency of the entire process.

3.3 Integration Time

The integration time of the detector (how long readings of the photon count are taken for) is one of the easiest parameters to vary while carrying out the procedure in order to optimise it. As such,

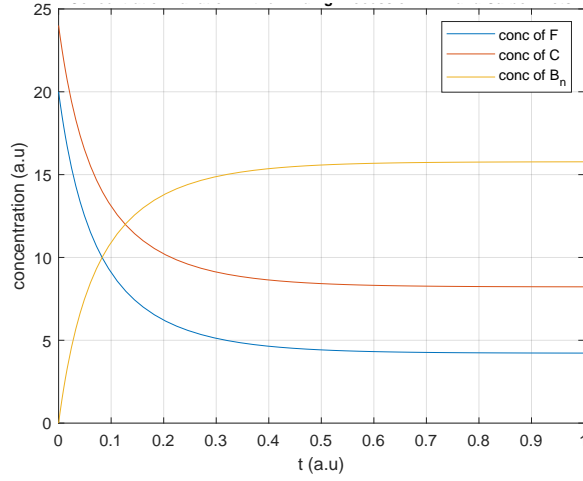


Figure 6: Numerical solution of ODEs in eq.(2)-(4) assuming $f_0 = 20$, $c_0 = 24$ and $r_1 = 0.5$ and $r_{-1} = 1.1$ (arbitrary constants).

we examined how varying the integration time affected the results of our model.

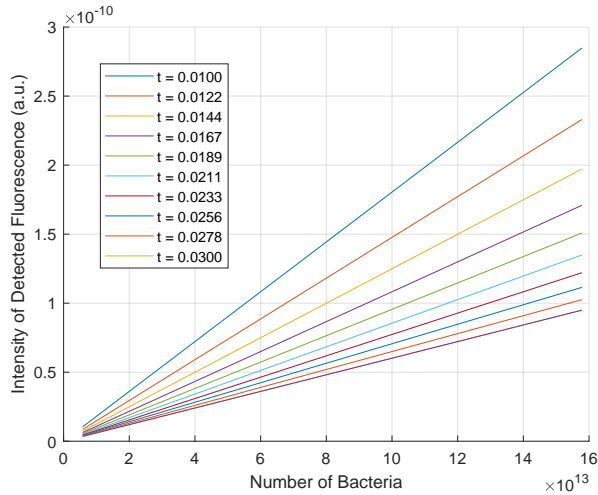


Figure 7: Fluorescence intensity detected against number of bacteria for arbitrary constants $k_1 = 1.2$, $k_2 = 1.1$, $c_0 = 3$ and n_{photon} values from data obtained. Ten values for integration time are equally spaced in the interval $[0.01, 0.03]$.

It can be seen in figure 7 that a larger integration time results in a lower intensity for the same number of bacteria present in the sample. As such, to avoid saturating the detector while analysing samples with large numbers of bacteria, a large integration time would be necessary. However, this would not work in practice as too large of an integration time would lead to photobleaching and would introduce too much noise into the detector.

3.4 Further Developments

One of the principle assumptions for this model is that the binding ratio is 1:1. Consequently, the steady-state values would be altered and we could not optimise the number of carbon nano-dots for a bacterial sample. However, this assumption does enable us to simplify the dynamics to be understandable and manipulable. In future models, we could investigate how the stoichiometry in the binding process affects the dynamics.

Furthermore, using precise starting concentrations will reveal how the model behaves over a more realistic scale. We have also used some constants specific to *E.coli*, whereas other bacteria will have different binding affinities and number of fimbriae so the model would require modification to represent other bacterial infections.

4 Conclusion

In this paper, we have developed a suite of mathematical models to describe the binding process of bacteria to the carbon nano-dots developed in the Nanoplex platform by Fluoretiq. The models show a fluid progression of modelling the fluorescence dynamics from a simple photocycle to a more generic model describing any potential photobleaching in the system. We also modelled the concentration of bacteria in simulated assays set up during the diagnostic process. The analysis was performed either by solving the systems of ODEs analytically, examining the steady state nature of the system, or by fitting curves to the data obtained from Fluoretiq. This allowed us to understand how bacteria is detected in the Nanoplex platform through a set of varying parameters.

The model of the binding process revealed that the concentrations of the reactants and products reach a steady state over a large time frame. This time frame was closely linked to the rates of reaction (r_1 and r_{-1}), which in turn were determined by the association and dissociation rates between the carbon nano-dots and the fimH proteins. The main limitation of our model is the assumption that there exists a 1:1 ratio between the reactants, which simplified our model, yet may be unrealistic.

We first developed a simple model of the fluorescence process, treating it as a reversible reaction before using the law of mass action to derive a system of ODEs describing the relative concentrations of excited and non-excited molecules. The intensity of fluorescence is then determined by the concentration of excited molecules. In our second model of fluorescence, taking reference from Jablonski's diagram, we added an intermediate state to allow for internal conversion. Additionally, we accounted for the effects of possible photobleaching by adding an absorption term representing the destruction of molecules.

By taking our second model of the photokinetics of the fluorescence process and comparing the dynamics resulting from our model to that of [15], we determined that the intensity of fluorescence is proportional to the concentration of bound molecules. We fit our proportional model to data to estimate the constant of proportionality ($\Omega = 2.3729 \times 10^3$). Then, by using the steady state solutions of our ODEs describing the binding process, the intensity of fluorescence detected was directly related to the initial concentration of fimH, from which the number of bacteria can be simply calculated. Hence, given that the rate constants of the binding process are known, for any intensity detected, the number of bacteria present in the sample can be found.

References

- [1] Chasteen, T. G. (2013). Jablonski diagram. <https://tinyurl.com/jablonskiDIAGRAM>.
- [2] Cooper, O., Eftekhari, E., Carter, J., Mallard, B., Kaur, J., Kiefel, M. J., Haselhorst, T., Li, Q., and Tiralongo, J. (2020). Fluorescent carbon dots functionalized with self-assembled glycan monolayers for probing interactions across the glyco-interactome. *ACS Applied Nano Materials*, 3(8):7804–7817.
- [3] Dellit, T. H., Owens, R. C., McGowan, J. E., Gerding, D. N., Weinstein, R. A., Burke, J. P., Huskins, W. C., Paterson, D. L., Fishman, N. O., Carpenter, C. F., et al. (2007). Infectious diseases society of america and the society for healthcare epidemiology of america guidelines for developing an institutional program to enhance antimicrobial stewardship. *Clinical Infectious Diseases*, 44(2):159–177.
- [4] Fellers, T., Vogt, K., and Davidson, M. (2020). Ccd signal-to-noise ratio. <https://tinyurl.com/NikonCCD>.
- [5] Filice, G. A., Drekonja, D. M., Thurn, J. R., Hamann, G. M., Masoud, B. T., and Johnson, J. R. (2015). Diagnostic errors that lead to inappropriate antimicrobial use. *Infection Control & Hospital Epidemiology*, 36(8):949–956.
- [6] Flynn, J. H. and Morrow, W. L. (1964). Photolysis of cellulose in a vacuum with 2537 a. light. *Journal of Polymer Science Part A: General Papers*, 2(1):81–89.
- [7] Hecker, M. T., Aron, D. C., Patel, N. P., Lehmann, M. K., and Donskey, C. J. (2003). Unnecessary use of antimicrobials in hospitalized patients: current patterns of misuse with an emphasis on the antianaerobic spectrum of activity. *Archives of internal medicine*, 163(8):972–978.
- [8] Helmenstine, A. M. (2019). Factors that affect the chemical reaction rate. <https://tinyurl.com/factors-affecting-reactions>.
- [9] Jovin, T. M. and Arndt-Jovin, D. J. (1989). FRET microscopy: Digital imaging of fluorescence resonance energy transfer. application in cell biology. In *Cell Structure and Function by Microspectrofluorometry*, pages 99–117. Elsevier.
- [10] Krogfelt, K. A. (1991). Bacterial Adhesion: Genetics, Biogenesis, and Role in Pathogenesis of Fimbrial Adhesins of Escherichia coli. *Reviews of Infectious Diseases*, 13(4):721–735.
- [11] L’Annunziata, M. F. (2003). Nuclear radiation, its interaction with matter and radioisotope decay. *Handbook of Radioactivity Analysis*, pages 1–122.
- [12] Martí Andrés, P., Escuder-Gilabert, L., Martín-Biosca, Y., Sagrado, S., and Medina-Hernández, M. (2015a). Simultaneous determination of pyridoxine and riboflavin in energy drinks by high-performance liquid chromatography with fluorescence detection. *Journal of Chemical Education*, 92:150212082216002.
- [13] Martí Andrés, P., Escuder-Gilabert, L., Martín-Biosca, Y., Sagrado, S., and Medina-Hernández, M. (2015b). Simultaneous determination of pyridoxine and riboflavin in energy drinks by high-performance liquid chromatography with fluorescence detection. *Journal of Chemical Education*, 92:150212082216002.
- [14] Nazir, R., Rehman, S., Nisa, M., and ali Baba, U. (2019). Exploring bacterial diversity: from cell to sequence. In *Freshwater Microbiology*, pages 263–306. Elsevier.

- [15] Pu, Y. and Alfano, R. (2013). Time-resolved fluorescence polarization spectroscopy and optical imaging of smart receptor-targeted contrast agents in tissues for cancer detection. In *Lasers for Medical Applications*, pages 368–392. Elsevier.
- [16] Slade, K. M., Steele, B. L., Pielak, G. J., and Thompson, N. L. (2009). Quantifying green fluorescent protein diffusion in escherichia coli by using continuous photobleaching with evanescent illumination. *The Journal of Physical Chemistry B*, 113(14):4837–4845.
- [17] Stricker, J., Maddox, P., Salmon, E., and Erickson, H. P. (2002). Rapid assembly dynamics of the escherichia coli ftsz-ring demonstrated by fluorescence recovery after photobleaching. *Proceedings of the National Academy of Sciences*, 99(5):3171–3175.
- [18] Thelwall, S. (2018). Clostridium difficile infection: mandatory surveillance 2017/18: Summary of the mandatory surveillance annual epidemiological commentary 2017/18. *Public Health England*, pages 1–7.
- [19] Waters, J. C. (2009). Accuracy and precision in quantitative fluorescence microscopy. *Journal of Cell Biology*, 185(7):1135–1148.
- [20] Wüstner, D., Christensen, T., Solanko, L., and Sage, D. (2014). Photobleaching kinetics and time-integrated emission of fluorescent probes in cellular membranes. *Molecules*, 19(8):11096–11130.

Appendix A Eigenvector and Eigenvalue Analysis for Fluorescence Photokinetics: Photobleaching Model

Eigenvectors matrix:

$$\begin{bmatrix} \frac{k_2\sigma_5^2}{\sigma_1} + \sigma_6 - \frac{\sigma_2\sigma_5}{k_1\sigma_9} & \frac{k_2\sigma_4^2}{\sigma_1} + \sigma_6 - \frac{\sigma_2\sigma_4}{k_1\sigma_9} & \frac{k_2\sigma_3^2}{\sigma_1} + \sigma_6 - \frac{\sigma_2\sigma_3}{k_1\sigma_9} \\ \frac{\sigma_5^2}{\sigma_9} + \sigma_7 - \frac{(k_1k_2k_3)\sigma_5}{\sigma_9} & \frac{\sigma_4^2}{\sigma_9} + \sigma_7 - \frac{(k_1k_2k_3)\sigma_4}{\sigma_9} & \frac{\sigma_3^2}{\sigma_9} + \sigma_7 - \frac{(k_1k_2k_3)\sigma_3}{\sigma_9} \\ 1 & 1 & 1 \end{bmatrix}$$

where,

$$\begin{aligned} \sigma_1 &= k_{-1}k_1^2 - k_1k_2^2 + k_{-1}k_1k_2 \\ \sigma_2 &= k_{-1}k_1 + k_1k_2 + k_{-1}k_2 + k_2k_3 \\ \sigma_3 &= \frac{2k_1}{3} + \frac{k_{-1}}{3} + \frac{k_3}{3} - \frac{\sigma_{11}}{2\sigma_{10}} + \frac{\sigma_{10}}{2} - \sigma_8 \\ \sigma_4 &= \frac{2k_1}{3} + \frac{k_{-1}}{3} + \frac{k_3}{3} - \frac{\sigma_{11}}{2\sigma_{10}} + \frac{\sigma_{10}}{2} + \sigma_8 \\ \sigma_5 &= \frac{2k_1}{3} + \frac{k_{-1}}{3} + \frac{k_3}{3} - \frac{\sigma_{11}}{\sigma_{10}} - \sigma_{10} \\ \sigma_6 &= \frac{k_2^3 + k_1k_{-1}k_3 + k_1k_2k_3 + k_{-1}k_2k_3}{k_1\sigma_9} \\ \sigma_7 &= \frac{k_2^2 + k_3k_2 + k_1k_3}{\sigma_9} \\ \sigma_8 &= \frac{\sqrt{3}(\frac{\sigma_{11}}{\sigma_{10}} + \sigma_{10})i}{2} \\ \sigma_9 &= -k_2^2 + k_{-1}k_2 + k_1k_{-1} \\ \sigma_{10} &= (\sqrt{(\frac{\sigma_{16}^3}{27} - \sigma_{12} + \sigma_{14} + \sigma_{13} - \sigma_{15})^2} + \sigma_{11}^3 - \frac{\sigma_{16}^3}{27} + \sigma_{12} - \sigma_{14} - \sigma_{13} + \sigma_{15})^{\frac{1}{3}} \\ \sigma_{11} &= \frac{2k_1k_3}{3} + \frac{k_{-1}k_3}{3} - \frac{\sigma_{16}^2}{9} + \frac{k_1^2}{3} + \frac{k_2^2}{3} \\ \sigma_{12} &= \frac{\sigma_{16}(k_1^2 + 2k_1k_3 + k_2^2 + k_{-1}k_3)}{6} \\ \sigma_{13} &= \frac{k_1^2k_3}{2} \\ \sigma_{14} &= \frac{k_1k_2^2}{2} \\ \sigma_{15} &= \frac{k_1k_{-1}k_2}{2} \\ \sigma_{16} &= 2k_1 + k_{-1} + k_3 \end{aligned}$$

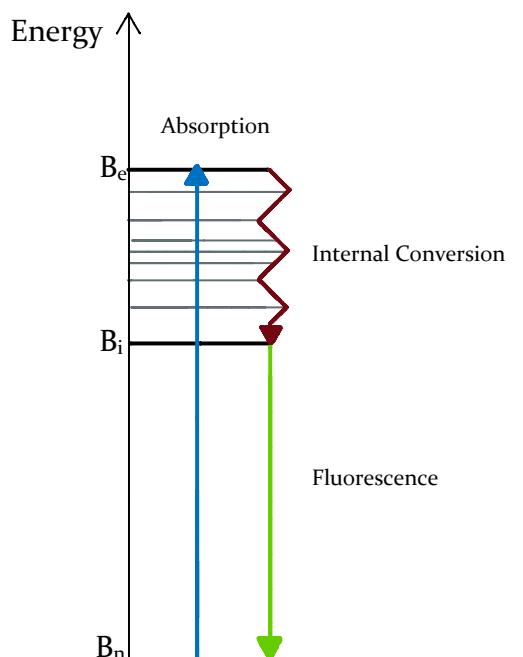
Eigenvalues matrix:

$$\begin{bmatrix} \sigma_2 - \frac{k_{-1}}{3} - \frac{k_3}{3} - \frac{\sigma_3}{\sigma_2} - \frac{2k_1}{3} & 0 & 0 \\ 0 & \frac{\sigma_3}{2\sigma_2} - \frac{k_{-1}}{3} - \frac{k_3}{3} - \frac{2k_1}{3} - \frac{\sigma_2}{2} - \sigma_1 & 0 \\ 0 & 0 & \frac{\sigma_3}{2\sigma_2} - \frac{k_{-1}}{3} - \frac{k_3}{3} - \frac{2k_1}{3} - \frac{\sigma_2}{2} + \sigma_1 \end{bmatrix}$$

where,

$$\begin{aligned} \sigma_1 &= \frac{\sqrt{3}(\frac{\sigma_3}{\sigma_2} + \sigma_2)i}{2} \\ \sigma_2 &= (\sqrt{(\frac{\sigma_3^3}{27} - \sigma_4 + \frac{k_1k_2^2}{2} + \frac{k_1^2k_3}{2} - \frac{k_1k_{-1}k_2}{2})^2} + \sigma_3^3 - \frac{\sigma_3^3}{27} + \sigma_4 - \frac{k_1k_2^2}{2} - \frac{k_1^2k_3}{2} + \frac{k_1k_{-1}k_2}{2})^{\frac{1}{3}} \\ \sigma_3 &= \frac{2k_1k_3}{3} + \frac{k_{-1}k_3}{3} - \frac{\sigma_5^2}{9} + \frac{k_1^2}{3} + \frac{k_2^2}{3} \\ \sigma_4 &= \frac{\sigma_5(k_1^2 + 2k_1k_3 + k_2^2 + k_{-1}k_3)}{6} \\ \sigma_5 &= 2k_1 + k_{-1} + k_3 \end{aligned}$$

Appendix B Jablonski's Diagram



Appendix C EDI Evaluation

There may not seem to be any obvious underlying ethical implications with the analysis of a urine sample however there are a few important factors to consider. As with any medical process we must respect that everyone legally has the right to doctor-patient confidentiality; a doctor may not discuss anything said between themselves and a patient unless strictly specified. This has consequently made it difficult to access data on which to test our model. Fortunately, since ours is a theoretical mathematical model, this has not been a notable issue in terms of the theory or assumptions behind our equations. However further testing must be carried out with further data only available to doctors before our model sees any real world application.

As previously mentioned, those taking pregnancy supplements or vitamin supplements, perhaps for an underlying health condition, may change the makeup of the urine sample and lead to a higher concentration of naturally occurring fluorophores. It is therefore important to determine the noise due to autofluorescence individually for every patient rather than relying on data taken over an average of patients. This ensures everyone has access to this method of diagnosis and it is as inclusive as possible.

Appendix D COVID-19 Mitigation

Doing any project during COVID is made more difficult because you can not meet up as easily with your group to discuss and present ideas to one another. To combat this problem, we made a team on Microsoft Teams that we would share any relevant documentation into and held meetings on this too.

Some members were in an isolation period whilst the project was going on, due to either a positive test or having come into contact with someone who had the virus. Due to this, we sometimes could not all attend the meetings, leading to some of the group members not fully keeping up to date with the progress that had been made at the meeting. For the members that had received a positive test, we could not do as much work as we would hope to do during this isolation period due to the effects of the virus.

Due to the fact that all meetings were completed at home remotely, sometimes the efficiency of these meetings was affected by the quality of internet connection that group members were experiencing. Occasionally, some of us could not join parts of the meeting because the internet connection could not support the call. We did solve these problems however, by making sure we held catch up meetings, to discuss any progress that had been made in the past week.